AIAA 81-0114R

Application of Adaptive Grids to Fluid-Flow Problems with Asymptotic Solutions

M. M. Rai* and D. A. Anderson†
Iowa State University, Ames, Iowa

Proper grid point location is important in the asymptotic finite-difference solution of any fluid-flow or heat transfer problem. This paper uses a new technique that provides a simple way of moving the mesh points in physical space in order to reduce the error in the computed asymptotic solution relative to that obtained using a fixed mesh. Applications to fluid-flow problems are presented, including boundary-layer flow and inviscid supersonic flow over cylinders and wedges with associated detached shocks. The treatment of curved boundaries, stationary and nonstationary boundaries, and systems of partial differential equations is discussed. Significant error reductions are demonstrated.

Introduction

THE accuracy of the finite-difference solution of a partial differential equation is dependent upon the suitability of the grid used in computing the solution. It is clear that two solutions to the same problem will not have equal accuracy for the same number of mesh points if the points are located differently in each case. The typical grid point allocation problem in computational fluid dynamics may be stated in the following way: If a solution to a set of partial differential equations is required on a physical domain subject to prescribed boundary conditions, how should a fixed number of grid points be distributed in order to assure that the solution obtained is the best? The term "best" as used here implies that some measure of error has been used in the point allocation. Since the size and complexity of the typical problem attempted using computational methods have increased dramatically, it is imperative that grid points be used as efficiently as possible to minimize storage requirements.

The construction of finite-difference grid systems has received a great deal of attention over the past five years. Several techniques have been proposed for producing acceptable body-fitted mesh systems. Probably the most well known of these methods is that of Thompson et al.,[1,2] in which a solution of Laplace's equation produces the grid in physical space. This technique is ideally suited to elliptic problems where a grid point allocation can be completed at the beginning of the calculation. Hindman et al.[3] produced an adaptive grid scheme for time-dependent flows. The grid speeds in physical space were obtained by using the idea proposed by Thompson, Thames, and Mastin but, in addition, differentiating the equations for physical grid point location with respect to time. At each time step, a matrix inversion led to expressions for the components of the grid point velocity. Unfortunately, Hindman's work included only the effect of boundary motion on the grid speeds.

The technique used to determine grid point motion in the present study is that proposed by Rai and Anderson.[4] The influence of both boundary motion and the details of the internal flowfield are included in the calculation of the grid point distribution. Numerical solutions for a number of fluid-flow problems are presented showing the applicability of the technique to both viscous and inviscid flows. These examples include laminar boundary-layer flow over a flat plate, inviscid supersonic flow over a cylinder, and inviscid supersonic flow over a pointed wedge, both of the latter with a detached shock.

Grid Point Motion

The method used for adjusting the physical grid point location has already been discussed in detail in Ref. 4 and only a brief summary of the main ideas will be given in this section. Given a certain number of mesh points, the error in the computed solution can be minimized by allocating more points to regions of large truncation error and fewer points to the regions of small truncation error. This can be done if points in large-error regions attract other points and points in low-error regions repel other points. It is also logical to assume that the further a point A is from a point B, the smaller the effect of point A on B. In one space dimension where the physical coordinates are (x,t) and the computational coordinates are (ξ,τ), the above considerations result in an equation of the form

$$(\xi_i)_\tau = K\left\{ \sum_{j=i+1}^{N} \frac{|e|_j - |e|_{\text{av}}}{r_{i,j}^n} - \sum_{j=1}^{i-1} \frac{|e|_j - |e|_{\text{av}}}{r_{i,j}^n} \right\} \quad (1)$$

$$(x_\tau)_i = (\xi_i)_\tau / (\xi_x)_i \qquad i=2,3,\ldots,N-1$$

where $(\xi_i)_\tau$ is the speed of the grid point in computational space, K and n are constants, N is the total number of grid points, $r_{i,j}$ is the distance between points i and j in computational space, $|e|_j$ is the absolute value of the truncation error at point j, and $|e|_{\text{av}}$ is the average of $|e|_j$ over all points.

In two dimensions where the physical coordinates are given by (x,y,t) and the computational coordinates by (ξ,η,τ), the quantities $(\xi_{i,j})_\tau$ and $(\eta_{i,j})_\tau$ take the form

$$(\xi_{i,j})_\tau = K_1 \sum_{\ell=1}^{M} \left[\sum_{k=i+1}^{N} \frac{|e^\xi|_{k,\ell} - |e^\xi|_{\text{av}_\ell}}{r^n} - \sum_{k=1}^{i-1} \frac{|e^\xi|_{k,\ell} - |e^\xi|_{\text{av}_\ell}}{r^n} \right]$$

$$(\eta_{i,j})_\tau = K_2 \sum_{k=1}^{N} \left[\sum_{\ell=j+1}^{M} \frac{|e^\eta|_{k,\ell} - |e^\eta|_{\text{av}_k}}{r^n} - \sum_{\ell=1}^{j-1} \frac{|e^\eta|_{k,\ell} - |e^\eta|_{\text{av}_k}}{r^n} \right]$$

$$r = \sqrt{(i-k)^2 + (j-\ell)^2} \quad (2)$$

Presented as Paper 81-0114 at the AIAA 19th Aerospace Sciences Meeting, St. Louis, Mo., Jan. 12-15, 1981; submitted March 10, 1981; revision received Sept. 8, 1981.

*Graduate Assistant, Department of Aerospace Engineering and Computational Fluid Dynamics Institute.

†Professor, Department of Aerospace Engineering, and Director, Computational Fluid Dynamics Institute. Member AIAA.

where K_1, K_2, and n are constants, N the number of points in the ξ direction, and M the number of points in the η direction. The quantities e^{ξ} and e^{η} are the errors in the ξ and η directions, respectively. Points lying along a constant η line can be made to move tangential to this line by equating $(\eta_{i,j})_\tau$ to zero for all these points. A similar procedure is adopted for constant ξ lines. In the case of a curved stationary boundary, it is necessary to apply a small correction after the point is moved in order to bring it back to the boundary. However, if the boundary is stationary and also a straight line, no correction is necessary since the points move tangential to the boundary. In the case of a constantly self-correcting moving boundary such as a shock, once again no correction is necessary. The calculation of boundary-point speeds is discussed in detail in Ref. 4.

Results

The present technique has been used to generate the grids used in solving the one- and two-dimensional unsteady viscous Burgers' equation. The results of this investigation can be found in Ref. 4. The present paper will concentrate on the application of the adaptive grid technique to fluid-flow problems.

The first problem solved was that of the laminar boundary layer over a flat plate. The equations of continuity and conservation of momentum are

$$u_x + v_y = 0, \qquad uu_x + vu_y = \nu u_{yy} \tag{3}$$

In order for the boundary layer to have a constant thickness in the computational plane (only then is it possible for the grid to achieve steady state), a similarity transformation of the type

$$\xi = x, \quad \eta = (y/x)\,(Re_x)^{1/2}, \quad Re_x = (U_\infty x)/\nu \tag{4}$$

is first carried out. This transforms Eqs. (3) to

$$\xi u u_\xi + \left(\nu Re_x^{1/2} - \frac{u\eta}{2}\right) u_\eta = U_\infty u_{\eta\eta}$$

and

$$\xi u_\xi - (\eta/2)\,u_\eta + Re_x^{1/2} v_\eta = 0 \tag{5}$$

with the boundary conditions

$$u(\xi,0) = 0, \qquad v(\xi,0) = 0, \qquad u(\xi,\infty) = U_\infty \tag{6}$$

where U_∞ is the freestream velocity. A second transformation of the type

$$\alpha = \xi, \qquad \beta = \beta(\xi,\eta) \tag{7}$$

from the coordinates (ξ,η) to the computational coordinates (α,β) is now implemented. The transformed equations are now integrated in the computational space until the steady state is reached.

A fully implicit method was used to solve the problem. The method is first-order accurate in the marching direction α and second-order accurate in the transverse direction β. Three-point central differences were used to calculate the metrics of the transformation in the interior of the region and three-point backward and forward differences were used to calculate the metrics at the end points.

The error in the computed solution is determined using the "exact" Blasius solution. Figure 1 shows the results obtained with $\nu = 1.6 \times 10^{-4}$. The measure of the local truncation error e was taken to be

$$e \propto \mathrm{d}\eta^2 u_\eta \tag{8}$$

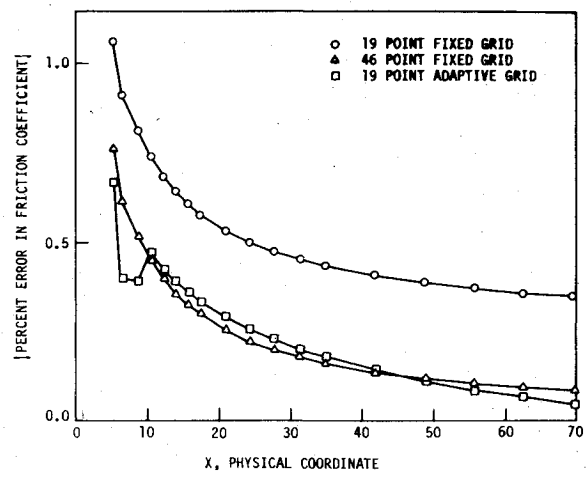

Fig. 1 Comparison of errors for the laminar boundary layer over a flat plate.

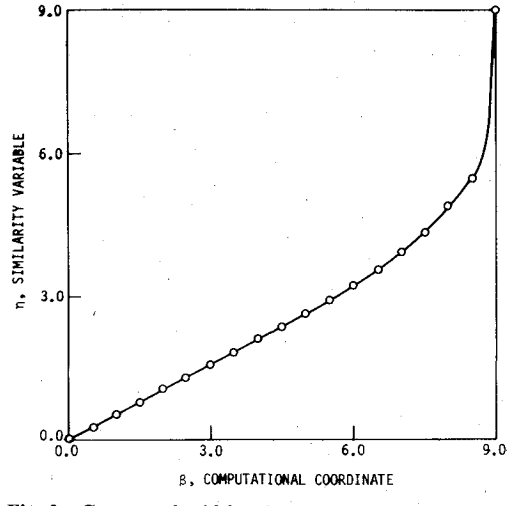

Fig. 2 Converged grid for the boundary-layer problem.

or

$$e \propto u_\beta/\beta_\eta \tag{9}$$

Figure 1 shows the error in the friction coefficient using 19 and 46 point equally spaced grids and a 19 point adaptive grid. The error in the 19 point fixed-grid solution is seen to be substantially reduced when a 19 point adaptive grid is used. The 19 point adaptive grid is found to decrease the percent error of the fixed-grid solution by a factor of seven at the last integration step. Figure 2 shows the transformation obtained with the adaptive grid. The grid is smooth and uniform.

The second problem for which results are presented is that of a cylinder in a supersonic freestream ($M_\infty = 2$) with an associated bow shock. The unsteady inviscid equations of motion are integrated in time until the steady state is reached. A boundary shock-fitting approach is used in conjunction with the SCM finite-difference method.[5] Results were obtained with 10×10 fixed‡ and adaptive grids. These results are compared to a 19×19 fixed-grid solution. The 19×19 fixed grid was generated by equally spacing points along the cylinder, drawing straight lines perpendicular to the cylinder through these points to meet the shock, and then dividing each ray between the shock and the body into equal segments.

‡The term "fixed" as used here and in the rest of the text implies that point motion is due only to the motion of the shock.

The region of interest does not possess any large error subregions. However, the problem does exhibit certain complexities in grid generation that have not been treated before, namely,

1) The presence of curved boundaries.
2) The nonstationary nature of one of the boundaries.
3) The solution of a system of partial differential equations.
4) The absence of any one predominant dependent variable that can be used to drive the grid.

The Euler equations in two dimensions can be written in the form

$$W_t + AW_x + BW_y = 0 \tag{10}$$

where

$$W = \begin{bmatrix} \rho \\ u \\ v \\ p \end{bmatrix} \quad A = \begin{bmatrix} u & \rho & 0 & 0 \\ 0 & u & 0 & \rho^{-1} \\ 0 & 0 & u & 0 \\ 0 & \gamma p & 0 & u \end{bmatrix}$$

$$B = \begin{bmatrix} v & 0 & \rho & 0 \\ 0 & v & 0 & 0 \\ 0 & 0 & v & \rho^{-1} \\ 0 & 0 & \gamma p & v \end{bmatrix} \tag{11}$$

and ρ is the density, u the velocity in the x direction, v the velocity in the y direction, p the pressure, and γ the ratio of specific heats. On making the transformation

$$\tau = t, \qquad \xi = \xi(x,y,t), \qquad \eta = \eta(x,y,t) \tag{12}$$

Equation (10) transforms into

$$W_\tau + \hat{A}W_\xi + \hat{B}W_\eta = 0 \tag{13}$$

where

$$\hat{A} = \xi_t I + \xi_x A + \xi_y B, \quad \hat{B} = \eta_t I + \eta_x A + \eta_y B \tag{14}$$

and I is the identity matrix. Assuming the error in the transformation metrics is negligible, we can write

$$e(W_\tau) = -\hat{A}e(W_\xi) - \hat{B}e(W_\eta) \tag{15}$$

where $e(W_\tau)$, $e(W_\xi)$, and $e(W_\eta)$ are the errors in computing W_τ, W_ξ, and W_η.

$$|e(W_\tau)| \le |\hat{A}e(W_\xi)| + |\hat{B}e(W_\eta)| \tag{16}$$

We let

$$e^\xi = |\hat{A}e(W_\xi)|, \qquad e^\eta = |\hat{B}e(W_\eta)| \tag{17}$$

where the norm used is the ℓ^1 norm and e^ξ and e^η are the errors that produce grid motion in the ξ and η directions.

The finite-difference method used to solve the problem is second-order accurate everywhere except at the surface boundary and is, hence, formally first-order accurate. The second derivative of W is a good estimate of the truncation error for first-order methods. Therefore, we get

$$e(W_\xi) \propto W_{\xi\xi}, \qquad e(W_\eta) \propto W_{\eta\eta} \tag{18}$$

Substituting Eq. (18) into Eq. (17) we get

$$e^\xi = |\hat{A}W_{\xi\xi}|, \qquad e^\eta = |\hat{B}W_{\eta\eta}| \tag{19}$$

In the above analysis we have assumed that the errors in the transformation metrics are negligible. This assumption is valid if excessive stretching of the mesh is prevented. In this problem the Jacobian of the transformation at every point is calculated initially ($J^1_{i,j}$) and stored. At every time step we calculate

$$\begin{aligned} R_{i,j} &= J^k_{i,j}/J^1_{i,j} \text{ if } J^k_{i,j}/J^1_{i,j} > 1 \\ &= J^1_{i,j}/J^k_{i,j} \text{ if } J^k_{i,j}/J^1_{i,j} < 1 \end{aligned} \tag{20}$$

where $J^k_{i,j}$ is the Jacobian at point i,j at the kth time step. Let

$$(R_{i,j})_{\max} = \max(R_{i,j}) \text{ over all points}$$

If $(R_{i,j})_{\max}$ exceeds a certain prescribed value $R_{\max}$, the grid speed is exponentially damped as follows:

$$\begin{aligned} (\xi_{i,j})_\tau^{\text{actual}} &= (\xi_{i,j})_\tau^{\text{calculated}} \times D \\ (\eta_{i,j})_\tau^{\text{actual}} &= (\eta_{i,j})_\tau^{\text{calculated}} \times D \\ D &= \exp\{-\text{const}[(R_{i,j})_{\max}/R_{\max}]^2\} \end{aligned} \tag{21}$$

The damping factor D gives us a strong control over the amount of grid point motion. It prevents both excessive stretching and excessive compressing of the grid.

Figure 3 shows the 10×10 fixed grid that serves as the initial position for the adaptive grid. A value of $R_{\max}$ of 1.03 was used for the adaptive grid. The final converged grid was very similar to the initial grid due to the very low value of $R_{\max}$. Figures 4-6 show the deviation of the dependent variables from the 19×19 grid point solution along the surface of the cylinder as a function of the angle θ (Fig. 3). The deviation in any representative physical quantity S is defined as

$$\text{deviation} = |S_{19\times19} - S_{10\times10}|$$

Figure 4 presents the deviation in the pressure. The 10×10 adaptive grid yields a much lower deviation than the 10×10 fixed grid. Figure 5 shows the deviation in the density. The adaptive grid yields a deviation that is again far smaller than

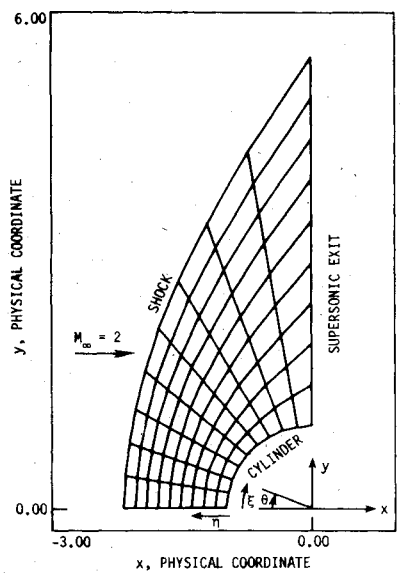

Fig. 3 Fixed grid for the cylinder in a supersonic freestream.

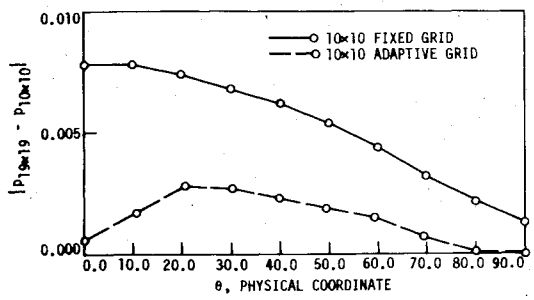

Fig. 4 Comparison of deviations in pressure for the cylinder.

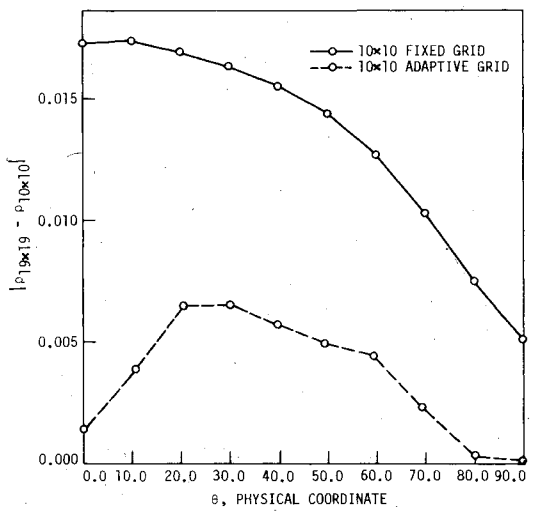

Fig. 5 Comparison of deviations in density for the cylinder.

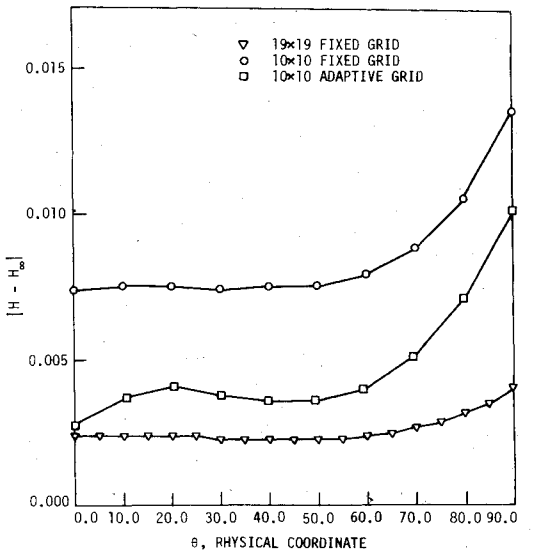

Fig. 6 Comparison of errors in total enthalpy for the cylinder.

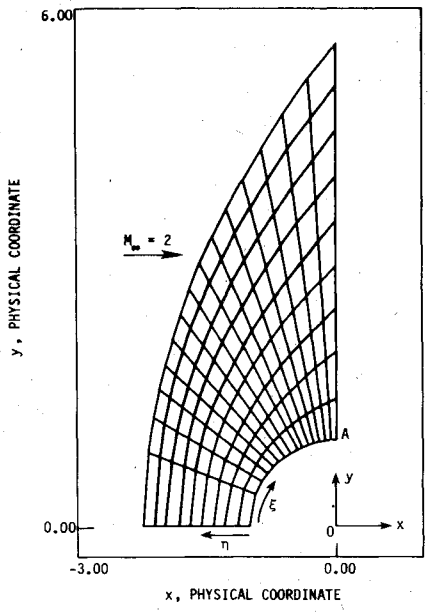

Fig. 7 Distorted initial grid for the cylinder.

that obtained with the fixed grid. Compared to the deviation in the density, the deviation in the velocity u was an order of magnitude smaller and the deviation in the velocity v was two orders of magnitude smaller on the average. The use of the adaptive grid resulted in a very slight increase in the deviations in u and v.

The quantities e^{ξ} and e^{η} in Eqs. (19) are approximations to an overall measure of error. Therefore, the adaptive grid technique in its present form cannot yield a lower deviation in every dependent variable at every point in the flowfield. This is the reason for the slightly larger deviations in u and v that were mentioned earlier. It should also be noted that the differences in u and v are much smaller than those in the density. Hence, the density has a greater effect on grid point motion.

The total enthalpy is a good measure of the total error at a point since it is a combination of all the other dependent variables. It is also known exactly at every point in the steady flowfield. Figure 6 shows the error in the total enthalpy plotted as a function of θ. The error in the 10×10 adaptive grid solution is seen to be much closer to the error in the 19×19 fixed grid solution than that obtained using a 10×10 fixed grid.

The deviation in the shock standoff distance with a 10×10 adaptive grid was 3.8% and that with a 10×10 fixed grid was 5.1%. The use of the adaptive grid did not affect the convergence rate for this problem.

The initial grid shown in Fig. 3 was found to be very close to the converged error-reducing grid obtained using the adaptive grid scheme. However, the adaptive grid is tolerant of relatively poor initial grids. This is extremely advantageous since the initial grid can be generated by any method without giving much importance to the characteristics of the flowfield. The adaptive grid scheme will then improve the initial point distribution. In order to illustrate this property of the adaptive grid, the point distribution shown in Fig. 7 was used as an initial grid. The grid contains 16 points along the body and 10 points normal to the body. The lack of sufficient points in the ξ direction in the region of the stagnation point and in the η direction in the region of point A makes this point distribution a poor initial grid. A calculation of the flowfield using the grid shown in Fig. 7 without the help of an adaptive grid yielded very inaccurate results.

The use of the adaptive grid scheme with a value of $R_{\max}$ of 6.0 resulted in the grid shown in Fig. 8. The clustering of grid points in the ξ direction near the stagnation point and in the η direction near the point A is evident. The error in total enthalpy obtained using the 16×10 adaptive grid was much smaller than that obtained using a 19×19 fixed grid. Hence, a comparison was made using the results obtained with a 31×21 fixed grid which was generated in the same way as the 19×19 fixed grid. The results of the comparison are shown in Fig. 9. The 16×10 adaptive grid yields a total enthalpy distribution along the body that is comparable to that ob-

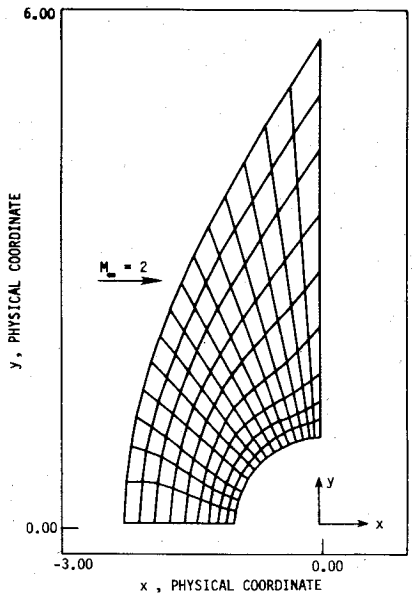

Fig. 8 Converged adaptive grid for the cylinder.

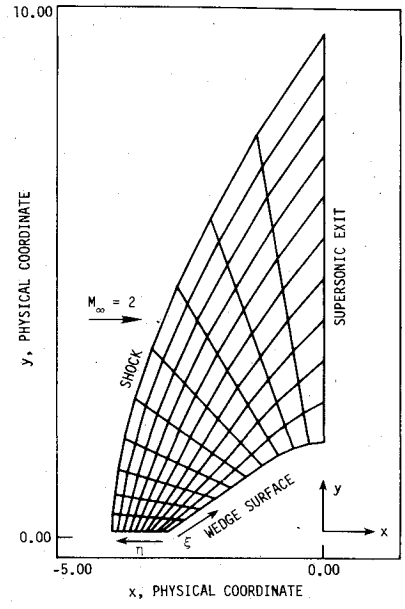

Fig. 11 Fixed grid for the wedge in a supersonic freestream.

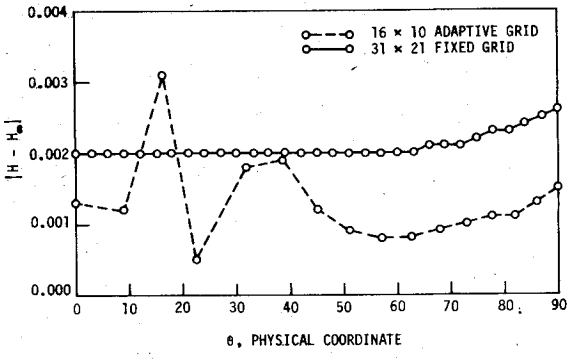

Fig. 9 Comparison of errors in total enthalpy for the cylinder.

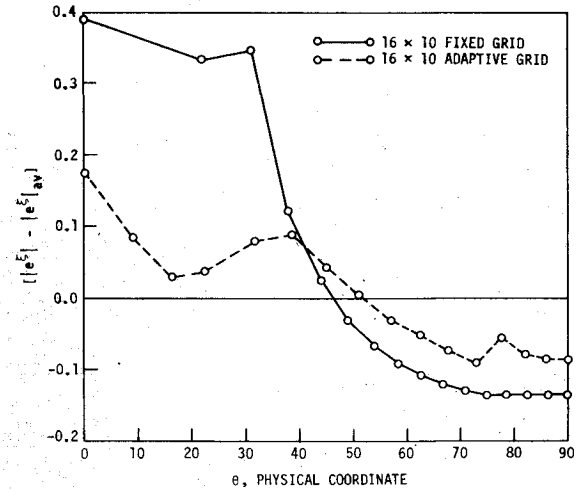

Fig. 10 Distribution of local truncation error along the surface of the cylinder.

tained using a 31×21 fixed grid. Figure 10 shows the distribution of the difference of the local error and the average error obtained along the body, with and without an adaptive grid. The use of the adaptive grid results in a more equitable distribution of local truncation error. This explains the very small errors in total enthalpy obtained using an adaptive grid.

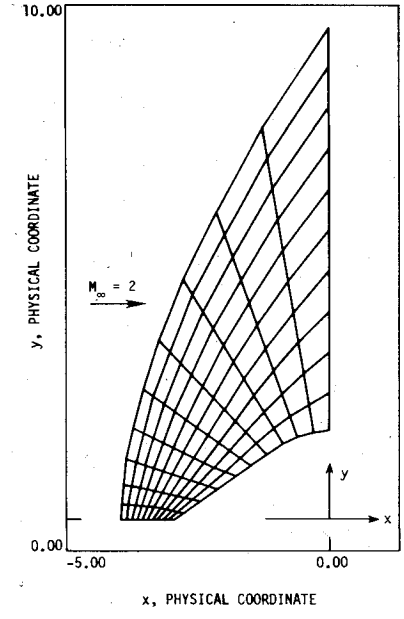

Fig. 12 Converged adaptive grid for the wedge in a supersonic freestream.

The third problem solved was that of a wedge in a supersonic freestream ($M_\infty = 2$) with the associated bow shock. Unlike the cylinder, the wedge has large gradients of the dependent variables at the tip and the shoulder (depending on the radius of the shoulder). Therefore, it becomes critical to redistribute points so that neither of these high-gradient regions is affected by the clustering of points at the other. The finite-difference method and the boundary-fitting technique used to solve the problem, the measure of local truncation error, and the control over excessive point motion are all the same as in the case of the cylinder. Results were obtained with 11×11 adaptive and fixed grids. These results were compared with those obtained using a 19×19 fixed mesh.

Figure 11 shows the 11×11 fixed grid that serves as the initial mesh point distribution for the adaptive grid. Figure 12 shows the converged grid with $R_{\max} = 1.5$. A clustering of mesh points can be observed both in the area of the tip and the shoulder.

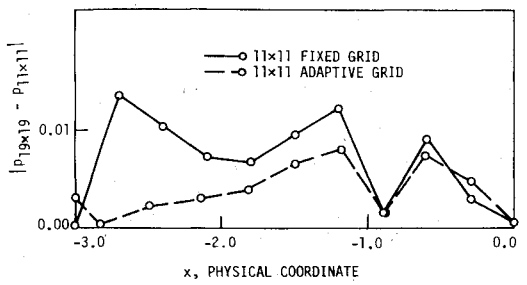

Fig. 13 Comparison of deviations in pressure for the wedge.

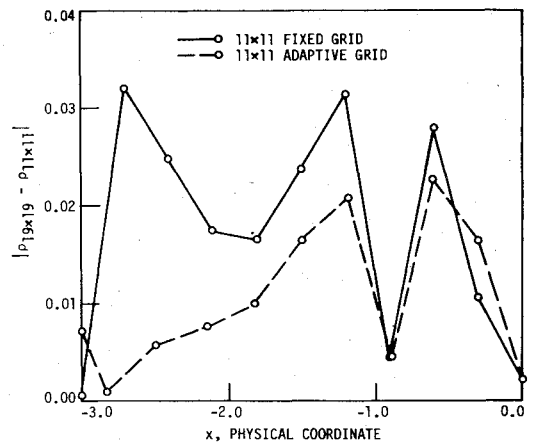

Fig. 14 Comparison of deviations in density for the wedge.

The tip of the wedge is at $x=-3$ and the point at the extreme right of the body is at $x=0$. Figures 13-15 show the deviation of the dependent variables from the 19×19 grid point solution as a function of x. The deviation for this problem is defined as

$$\text{deviation} = |S_{19\times19} - S_{11\times11}|$$

where S is some representative physical quantity. Figure 13 presents the deviation in the pressure. The 11×11 adaptive grid is seen to yield a much lower deviation than the 11×11 fixed grid. The deviation in the density is shown in Fig. 14. The decrease in the deviation with the use of an adaptive grid is evident. The deviations in u and v are comparable to the deviation in density for this problem. Unlike the cylinder, significant reductions in the deviations in u and v were obtained with the use of the adaptive grid. Figure 15 shows the error in the total enthalpy for all three grids. The error in the 11×11 adaptive grid solution is much smaller than the error obtained with an 11×11 fixed grid.

The deviation in the shock standoff distance was 2.2% for the adaptive grid and -3.8% for the fixed grid. In Fig. 16, the average shock velocity is plotted as a function of the iteration number. The adaptive grid solution was found to converge in 70% of the number of iterations required for convergence with a fixed grid.

Undetermined Constants

The equations governing grid point motion in two dimensions [Eqs. (2)] contain three undetermined constants, K_1, K_2, and n. The constants K_1 and K_2 can be determined by specifying the maximum grid velocities in the system $[(\xi_{i,j})_\tau]_{\max}$ and $[(\eta_{i,j})_\tau]_{\max}$ (Ref. 4). Very large values of $[(\xi_{i,j})_\tau]_{\max}$ and $[(\eta_{i,j})_\tau]_{\max}$ result in grid oscillations that die out slowly and very small values of these constants result in very slow grid convergence. The accuracy of the final solution was found to be relatively insensitive to the

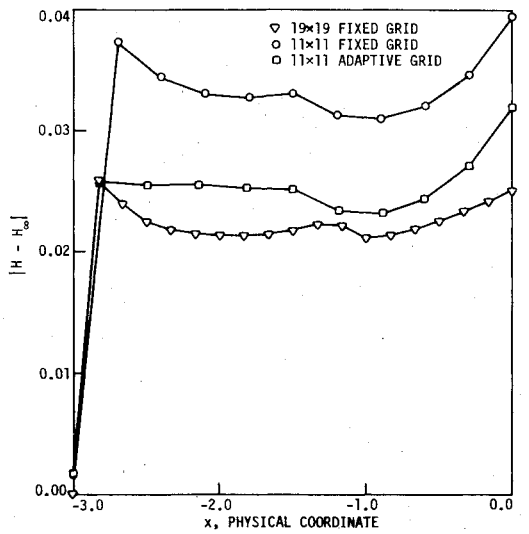

Fig. 15 Comparison of errors in total enthalpy for the wedge.

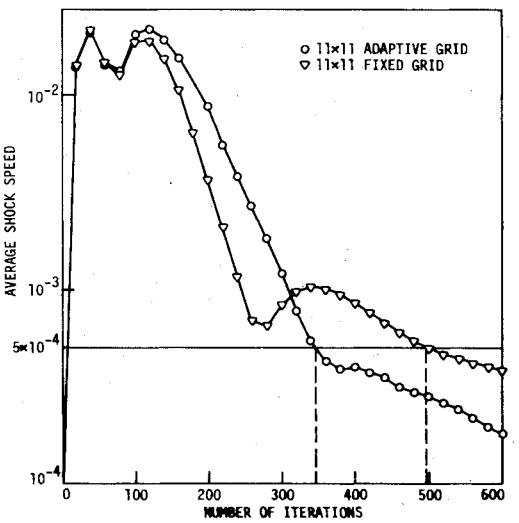

Fig. 16 Relative convergence rates for the cylinder.

maximum grid velocities in the range

$$0.1 \le [(\xi_{i,j})_\tau]_{\max},\quad [(\eta_{i,j})_\tau]_{\max} \le 5.0$$

The value used most often is unity.

It was found that for $R_{\max}=\infty$, the constant n had little effect on the final grid. It is advantageous to use large values of n in order to decrease the point cluster required to calculate the grid velocity at any point. However, for finite values of $R_{\max}$, a smoother grid is obtained for smaller values of n. This is because the point motion is smoother when larger clusters of grid points are used to calculate grid velocities. It has never been necessary to decrease n below two, and values of n up to seven have been used. A commonly used value of n is four.

Accurate measures of local truncation error generally involve the calculation of higher order derivatives of the dependent variables and the transformation metrics. The use of the computed solution and grid point locations in calculating these higher order derivatives results in very "noisy" error measures and, consequently, erratic point motion. The error measures used in this study involve only lower order derivatives and are hence smooth but inaccurate. The inaccuracy in the error estimate sometimes leads to excessive stretching or compressing of the grid. The point motion-controlling scheme given by Eqs. (20) and (21) prevents large distortions of the grid. Values of $R_{\max}$ close to

Table 1 Computing times

Problem	Type of grid	CPU time on CDC 6600, s
Flat plate	19 point fixed	5.78
	19 point adaptive	6.02
	46 point fixed	13.33
Cylinder	10×10 point fixed	79.49
	10×10 point adaptive	102.42
	19×19 point fixed	532.15
	16×10 point adaptive	382.34
	31×21 point fixed	1137.32
Wedge	11×11 point fixed	78.96
	11×11 point adaptive	76.14
	19×19 point fixed	500.45

unity will almost always result in a reduction in error. The maximum error reduction is obtained for the optimal R_{max}, which can only be obtained by a trial-and-error procedure. Even though the magnitude of the reduction in error depends on R_{max}, the adaptive grid, for a fairly accurate error measure, retains its error-reducing property for a range of R_{max} values. In the case of the wedge, the adaptive grid gave better solutions than the fixed grid for R_{max} up to 2.5. The best results were obtained for $R_{max} = 1.5$.

Time Requirements

Since the number of integration steps required for convergence with and without an adaptive grid is not always the same, time estimates will be given, both on a per integration step basis and a total computing time basis. For the boundary-layer problem, the generation of the grid and recalculation of the metrics took 50% of the time taken for integration. However, the results obtained are comparable to those obtained using a 46 point fixed grid. The 46 grid point solution takes 130% more computer time than the 19 point fixed grid solution. It should also be remembered that the equations being solved are very simple and a comparison based on percentages is not favorable to the adaptive grid technique.

In the case of the wedge and the cylinder, the generation of the grid took about 32% of the time taken for integration of the equations. It must be remembered that the solutions obtained using a adaptive grid converge in fewer integration steps. Table 1 gives the actual times used for the calculations.

Conclusion

A new method of generating adaptive grids for time-asymptotic solutions has been applied to a number of fluid dynamics problems. In calculating grid speed and final point location, both boundary motion and evolution of the solution of the internal flowfield are considered.

Results were presented for the laminar boundary layer over a flat plate, a cylinder in a supersonic freestream, and a wedge in a supersonic freestream. Significant error reductions in the dependent variables were demonstrated in all cases. The adaptive grid solutions were observed to converge faster than the fixed grid solutions for the wedge and cylinder problems. The results show the applicability of the adaptive grid technique to complex fluid-flow problems involving many dependent variables, curved stationary and moving boundaries, and systems of partial differential equations.

The effectiveness of the adaptive grid in reducing the error in the computed solution depends mainly on the accuracy with which local and global errors can be estimated. The inaccuracy in the error estimates necessitate the use of the point-motion controlling scheme and the specification of the arbitrary constant R_{max}. The development of better methods of establishing local errors will remove the need for the damping terms given by Eq. (21) and consequently the specification of R_{max}. Hence, future work will involve the estimation of local and global errors more accurately.

Acknowledgments

This work was sponsored by NASA under NASA Cooperative Agreement NCCI-17. The authors wish to acknowledge the encouragement and helpful suggestions provided during this investigation by Manuel Salas at NASA Langley Research Center.

References

[1] Thompson, J. F., Thames, F. C., and Mastin, C. W., "Automatic Numerical Generation of Body-Fitted Curvilinear Coordinate Systems for Fields Containing Any Number of Arbitrary Two-Dimensional Bodies," *Journal of Computational Physics,* Vol. 15, 1974, pp. 299-319.

[2] Thompson, J. F., Thames, F. C., and Mastin, C. W., "TOMCAT—A Code for Numerical Generation of Boundary-Fitted Curvilinear Coordinate Systems on Fields Containing Any Number of Arbitrary Two-Dimensional Bodies," *Journal of Computational Physics,* Vol. 24, 1977, pp. 274-302.

[3] Hindman, R. G., Kutler, P., and Anderson, D. A., "A Two-Dimensional Unsteady Euler-Equation Solver for Flow Regions With Arbitrary Boundaries," AIAA Paper 79-1465, July 1979.

[4] Rai, M. M. and Anderson, D. A., "Grid Evolution in Time Asymptotic Problems," to be published in *Journal of Computational Physics.*

[5] Chakravarthy, S. R., Anderson, D. A., and Salas, M. D., "The Split Coefficient Matrix Method for Hyperbolic Systems of Gas Dynamic Equations," AIAA Paper 80-0268, Jan. 1980.